Monatsh Chem (2011) 142:973–978
DOI 10.1007/s00706-011-0569-4

ORIGINAL PAPER

$La_3Pd_4Zn_4$ and $La_3Pt_4Zn_4$ with a different coloring of the $Gd_3Cu_4Ge_4$-type structure

Trinath Mishra · Christian Schwickert · Rainer Pöttgen

Received: 15 June 2011 / Accepted: 12 July 2011 / Published online: 11 August 2011

Abstract The intermetallic zinc compounds $La_3Pd_4Zn_4$ and $La_3Pt_4Zn_4$ were synthesized by induction melting of the elements in sealed tantalum tubes. The structures were refined from X-ray single-crystal diffractometer data: $Gd_3Cu_4Ge_4$ type, *Immm*, $a = 1{,}440.7(5)$, $b = 743.6(2)$, $c = 419.5(2)$ pm, $wR_2 = 0.0511$, 353 F^2 for $La_3Pd_4Zn_4$; and $a = 1{,}439.9(2)$, $b = 748.1(1)$, $c = 415.66(6)$ pm, $wR_2 = 0.0558$, 471 F^2 for $La_3Pt_4Zn_4$ with 23 variables per refinement. The palladium (platinum) and zinc atoms build up a three-dimensional polyanionic $[Pd_4Zn_4]$ (260–281 pm Pd–Zn) and $[Pt_4Zn_4]$ (260–279 pm Pt–Zn) network in which the lanthanum atoms fill cavities of CN 14 (6 Pd/Pt + 8 Zn for La1) and CN 12 (6 Pd/Pt + 6 Zn for La2), respectively. The copper position of the $Gd_3Cu_4Ge_4$ type is occupied by zinc and the two crystallographically independent germanium sites by palladium (platinum), a new coloring pattern for this structure type. Within the $[Pd_4Zn_4]$ and $[Pt_4Zn_4]$ the Pd2 and Pt2 atoms form Pd2–Pd2 (291 pm) and Pt2–Pt2 (296 pm) dumbbells. The structures of $La_3Pd_4Zn_4$ and $La_3Pt_4Zn_4$ are discussed with respect to the prototype $Gd_3Cu_4Ge_4$ and the Zintl phase $Sr_3Li_4Sb_4$. Temperature-dependent magnetic susceptibility measurements indicate diamagnetism for $La_3Pt_4Zn_4$ and Pauli paramagnetism for $La_3Pd_4Zn_4$.

Keywords Intermetallic compounds · Zinc · Crystal chemistry

T. Mishra · C. Schwickert · R. Pöttgen (✉)
Institut für Anorganische und Analytische Chemie,
Westfälische Wilhelms-Universität Münster,
Corrensstrasse 30, 48149 Munster, Germany
e-mail: pottgen@uni-muenster.de

Introduction

Ternary intermetallic compounds $RE_xT_yX_z$ (RE = rare-earth element, T = transition metal, X = element of the third, fourth, or fifth main group) have been intensively studied over the last 40 years with respect to phase analyses, crystal structures, and physical properties. For most families of compounds, i.e., borides, aluminides, gallides, etc., extensive review articles have been published in the *Handbook on the Physics and Chemistry of Rare Earths* [1].

Recent investigations have shown that the X component can be substituted by magnesium [2] or cadmium [3], leading to either isotypic compounds or new intermetallics with related structure types. So far more than 200 $RE_xT_yMg_z$ [2] and $RE_xT_yCd_z$ [3] compounds each have been reported. In principle, compounds with zinc as X component can form with equal valence electron concentration. The RE–T–Zn systems, however, have only been scarcely investigated. Most studies have been reported for the equiatomic compounds RETZn [4–6, and refs. therein]. Similar to the magnesium and cadmium compounds, the RETZn phases also crystallize with either the orthorhombic TiNiSi- or hexagonal ZrNiAl-type structure.

For several of the La–T–Zn and Ce–T–Zn systems with T = Co, Ni, Cu, complete isothermal sections have been studied [7–9, and refs. therein]. These phase analytical studies revealed a variety of intermetallic compounds with quite different structural features, e.g., cobalt-rich phases with ordered variants of $NaZn_{13}$, β-Th_2Zn_{17}, or $BaCd_{11}$ [10], zinc-rich compounds with $CeCr_2Al_{20}$- [11, 12] and $Ce_2Al_2Co_{15}$-type [13] structure, or the ordering variants $RE_2T_3Zn_{14}$ [14]. The outstanding compound within the family of $RE_xT_yZn_z$ intermetallics is the static mixed-valent phase Ce_2RuZn_4 [15, 16], which exhibits two crystallographically independent sites for trivalent and

Table 1 Crystallographic data and structure refinement for $La_3Pd_4Zn_4$ and $La_3Pt_4Zn_4$, $Gd_3Cu_4Ge_4$ type, space group *Immm*, $Z = 2$

Empirical formula	$La_3Pd_4Zn_4$	$La_3Pt_4Zn_4$
Molar mass/g mol^{-1}	1,103.81	1,458.57
Lattice parameters/pm	$a = 1{,}440.7(5)$	$a = 1{,}439.9(2)$
(Guinier powder data)	$b = 743.6(2)$	$b = 748.1(1)$
	$c = 419.5(2)$	$c = 415.66(6)$
Cell volume/nm^3	$V = 0.4494$	$V = 0.4477$
Crystal size/μm^3	$20 \times 30 \times 50$	$25 \times 40 \times 50$
Calculated density/g cm^{-3}	8.16	10.82
Max./min. transmission	0.289/0.243	0.608/0.306
Radiation	Ag K_α	Mo K_α
	($\lambda = 56.086$ pm)	($\lambda = 71.073$ pm)
Linear absorption coeff./mm^{-1}	16.9	86.6
F(000)	950	1,206
θ range/°	2–22	3–32
$h\ k\ l$ range	±19, ±9, ±5	±20, ±11, ±6
Total reflections	2,254	2,815
Independent reflections	353 ($R_{int} = 0.1980$)	471 ($R_{int} = 0.0847$)
Reflections with $I \geq 2\sigma(I)$	276 ($R_{sigma} = 0.0870$)	389 ($R_{sigma} = 0.0540$)
Data/parameters	353/23	471/23
Goodness of fit	1.024	0.928
R indices [$I \geq 2\sigma(I)$]	$R_1 = 0.0357$	$R_1 = 0.0270$
	$wR_2 = 0.0472$	$wR_2 = 0.0538$
R indices (all data)	$R_1 = 0.0525$	$R_1 = 0.0402$
	$wR_2 = 0.0511$	$wR_2 = 0.0558$
Extinction coefficient	0.0024(3)	0.00175(13)
Diff. Fourier residues/e$^-$ Å^{-3}	2.90 and −4.87	2.43 and −2.91

intermediate-valent cerium. Further interesting phases are the 1.7 K antiferromagnet CePtZn [17, 18], the heavy-fermion system YbPtZn [19], the 51 K ferromagnet EuAuZn [20], and the magnetocaloric Laves phase $EuRh_{1.2}Zn_{0.8}$ [21].

In the course of our systematic studies on the equiatomic REPtZn series [6] we obtained a new compound $La_3Pt_4Zn_4$ with a $Gd_3Cu_4Ge_4$-related [22] structure. The crystal chemistry and properties of $La_3Pt_4Zn_4$ and isotypic $La_3Pd_4Zn_4$ are reported herein.

Results and discussion

Structure refinement

Analyses of the diffractometer data sets revealed body-centered orthorhombic lattices and no further extinctions, leading to space groups *Immm*, *Imm*2, and *I*222, of which the centrosymmetric group was found to be correct during structure refinement. The structure of the palladium compound was determined first. The starting atomic positions were obtained from direct methods with SHELXS-97 [23], and the structure was refined using SHELXL-97 [24] (full-matrix least-squares on F^2) with anisotropic atomic displacement parameters for all sites. Adjustment of the refined composition and the Wyckoff sequence with the Pearson Crystal Data Base [25] readily revealed isotypism with $Gd_3Cu_4Ge_4$ [22]. In the following cycles both structures were refined with this setting. The occupancy parameters were then refined in a separate series of least-squares cycles. All sites were fully occupied within one standard deviation, and in the final cycles the ideal values were assumed again. The refinements converged to the values listed in Table 1. The final difference-Fourier syntheses revealed no significant residues. The refined atomic positions, anisotropic displacement parameters, and interatomic distances are given in Tables 2 and 3.

Crystal chemistry

The intermetallic zinc compounds $La_3Pd_4Zn_4$ and $La_3Pt_4Zn_4$ crystallize with the orthorhombic $Gd_3Cu_4Ge_4$-type [22] structure. So far, 70 compounds with this structural arrangement are listed in the Pearson data base [25]. Mainly $RE_3Cu_4(Si,Ge,Sn)_4$ and $RE_3Ag_4(Ge,Sn)_4$ tetrelides crystallize with this type. $La_3Pd_4Zn_4$ and $La_3Pt_4Zn_4$ are the first zinc compounds in this series.

Table 2 Atomic coordinates and anisotropic displacement parameters (pm^2) for $La_3Pd_4Zn_4$ and $La_3Pt_4Zn_4$

Atom	Wyckoff site	*x*	*y*	*z*	U_{11}	U_{22}	U_{33}	U_{12}	U_{eq}
$La_3Pd_4Zn_4$									
La1	2*d*	0	1/2	0	139(5)	119(7)	154(9)	0	137(3)
La2	4*e*	0.12896(5)	0	0	113(4)	179(5)	144(6)	0	145(3)
Pd1	4*f*	0.21539(7)	1/2	0	138(5)	291(9)	143(8)	0	191(4)
Pd2	4*h*	0	0.1954(2)	1/2	117(5)	133(7)	180(8)	0	143(3)
Zn	8*n*	0.32691(7)	0.1906(2)	0	172(5)	164(7)	200(9)	–60(5)	179(4)
$La_3Pt_4Zn_4$									
La1	2*d*	0	1/2	0	119(7)	99(6)	113(6)	0	110(3)
La2	4*e*	0.12687(8)	0	0	103(5)	132(4)	93(4)	0	109(2)
Pt1	4*f*	0.21694(5)	1/2	0	111(4)	169(3)	87(3)	0	122(2)
Pt2	4*h*	0	0.19768(8)	1/2	97(3)	104(3)	104(3)	0	102(2)
Zn	8*n*	0.32626(12)	0.19240(19)	0	135(8)	131(6)	141(6)	–40(5)	136(3)

U_{eq} is defined as one-third of the trace of the orthogonalized U_{ij} tensor. Coefficients U_{ij} of the anisotropic displacement factor tensor of the atoms are defined by: $-2\pi^2[(ha^*)^2U_{11} + \ldots + 2hka^*b^*U_{12}]$. $U_{13} = U_{23} = 0$

Projections of the $Gd_3Cu_4Ge_4$ and $La_3Pt_4Zn_4$ structures along the short unit cell axis are presented in Fig. 1. Both structures consist of three-dimensional $[Cu_4Ge_4]$ and $[Pt_4Zn_4]$ networks, however, with a different coloring [26], i.e., zinc on the copper and platinum on the germanium sites. This site exchange is in line with the course of the electronegativities of the respective elements. In view of the resulting different bonding situation, the two structures should be called isopointal [27, 28] rather than isotypic.

In the following discussion, when we quote interatomic distances, we refer to the $La_3Pt_4Zn_4$ structure. Within the $[Pt_4Zn_4]$ network, each zinc atom has distorted tetrahedral platinum coordination (Fig. 2) with Pt–Zn distances ranging from 260 to 279 pm, slightly larger than the sum of the covalent radii [29] of 254 pm. Similar range of Pt–Zn distances occurs for the distorted $ZnPt_{4/4}$ tetrahedra in CePtZn (268–273 pm) [17] and EuPtZn (265–271 pm) [20]. The $ZnPt_{4/4}$ tetrahedra share common corners and edges, and the two crystallographically independent lanthanum sites are coordinated by the triangular faces of these tetrahedra.

The bonding of the lanthanum atoms proceeds via shorter La–Pt contacts. The La–Pt distances range from 306 to 314 pm, only slightly longer than the sum of the covalent radii [29] of 298 pm. This bonding pattern is in line with the electronegativity differences between lanthanum and platinum. As is evident from the projection in Fig. 1, the two crystallographically independent lanthanum sites have markedly different coordinations. The La1 atoms fill relatively large cavities, while those for La2 are distinctly smaller. This is especially expressed by the much longer La1–Zn distances (356 pm) as compared with La2–Zn (317 and 321 pm). Such an extreme situation also occurs in the structure of $Yb_3Pd_4Ge_4$ [30], leaving the possibility of Yb^{II} (larger)/Yb^{III} (smaller) ordering.

The strong tilts of the $ZnPt_{4/4}$ tetrahedra lead to shorter Zn–Zn (288 pm) and Pt2–Pt2 (296 pm) distances within the three-dimensional $[Pt_4Zn_4]$ network. The Zn–Zn distance compares well with the structure of hcp zinc (6 × 266 and 6 × 291 pm), while the Pt–Pt distance is longer than in fcc platinum (277 pm) [31]. We can therefore assume only weakly bonding Pt–Pt interactions. In view of the highly electropositive character of lanthanum and zinc, one can safely ascribe a platinide character to these dumbbells. This is in line with the isopointal structures of the germanides and stannides, where Ge_2 and Sn_2 dumbbells occur.

Finally we compare the $La_3Pt_4Zn_4$ structure with the electron precise Zintl phases $Sr_3Li_4Sb_4$, $Ba_3Li_4Sb_4$ [32], and $Ba_3Li_4As_4$ [33]. As an example, a projection of the $Sr_3Li_4Sb_4$ structure is included in Fig. 1 (bottom). Antimony as the most electronegative component occupies the platinum positions of $La_3Pt_4Zn_4$, while the lithium and the alkaline-earth metal atoms take the zinc and lanthanum sites, respectively. Considering the dumbbell formation (282 pm Sb1–Sb1, similar to the Sb–Sb intralayer distance of 291 pm in the Sb_6 rings of elemental antimony [31]) one obtains an electron partitioning scheme $(3Sr^{2+})^{6+}(4Li^{+})^{4+}(2Sb^{3-})^{6-}(Sb_2)^{4-}$ for, e.g., $Sr_3Li_4Sb_4$. Such a drastic charge transfer is certainly not possible for $La_3Pt_4Zn_4$, where the 17 valence electrons per formula unit 'La_3Zn_4' cannot be accommodated by the four platinum atoms. Nevertheless, one can assume positively polarized lanthanum and zinc and negatively polarized platinum.

Summing up, comparison of the structures of $Gd_3Cu_4Ge_4$, $La_3Pt_4Zn_4$, and $Sr_3Li_4Sb_4$ shows that the three compounds show distinctly different site occupancies and thus different bonding peculiarities and one should classify them as isopointal rather than isotypic, although the three structures have the same space group type and Wyckoff sequence.

Table 3 Interatomic distances (pm) in the structures of $La_3Pd_4Zn_4$ and $La_3Pt_4Zn_4$

$La_3Pd_4Zn_4$				$La_3Pt_4Zn_4$			
La1	4	Pd2	308.7	La1	4	Pt2	307.2
	2	Pd1	310.3		2	Pt1	312.4
	8	Zn	355.3		8	Zn	355.7
	4	La2	415.6		2	La1	415.7
	2	La1	419.5		4	La2	416.3
La2	2	Pd1	307.1	La2	2	Pt1	306.2
	4	Pd2	315.6		4	Pt2	313.7
	4	Zn	317.8		4	Zn	317.3
	2	Zn	318.4		2	Zn	321.2
	1	La2	371.6		1	La2	365.4
	2	Pd1	392.1		2	Pt1	395.9
	2	La1	415.6		2	La2	415.7
	2	La2	419.5		2	La1	416.3
Pd1	4	Zn	260.4	Pt1	4	Zn	260.3
	2	Zn	280.6		2	Zn	278.8
	2	La2	307.1		2	La2	306.2
	1	La1	310.3		1	La1	312.4
	2	La2	392.1		2	La2	395.9
Pd2	2	Zn	263.4	Pt2	2	Zn	263.3
	1	Pd2	290.6		1	Pt2	295.8
	2	La1	308.7		2	La1	307.1
	4	La2	315.6		4	La2	313.7
Zn	2	Pd1	260.4	Zn	2	Pt1	260.3
	1	Pd2	263.4		1	Pt2	263.3
	1	Pd1	280.6		1	Pt1	278.8
	1	Zn	283.4		1	Zn	287.9
	2	Zn	317.7		2	Zn	314.4
	2	La2	317.8		2	La2	317.3
	1	La2	318.5		1	La2	321.2
	2	La1	355.3		2	La1	355.7

All distances within the first coordination shells are listed. Standard deviations are all ≤0.3 pm

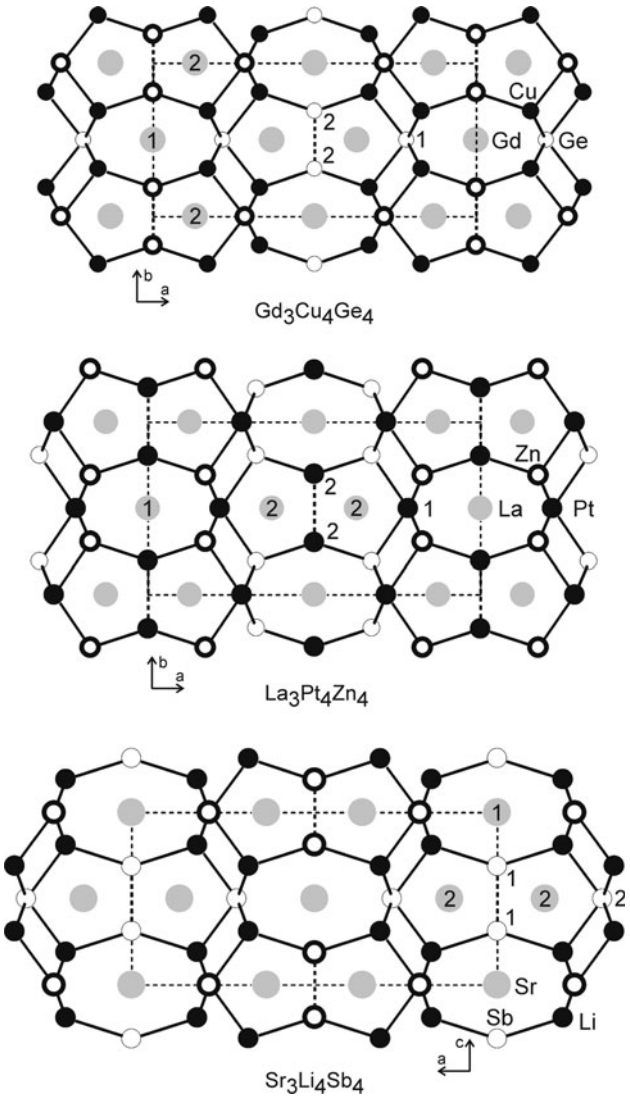

Fig. 1 Projections of the $Gd_3Cu_4Ge_4$, $La_3Pt_4Zn_4$, and $Sr_3Li_4Sb_4$ structures along the short unit cell axis. The three-dimensional $[Cu_4Ge_4]$, $[Pt_4Ge_4]$, and $[Li_4Sb_4]$ networks are emphasized. Atom designations and the crystallographically independent sites are marked

Magnetic properties

The temperature dependence of the magnetic susceptibility [$\chi(T)$ data] of $La_3Pt_4Zn_4$ measured in a field of 10 kOe is shown in Fig. 3. In the temperature range of 50–300 K, $La_3Pt_4Zn_4$ displays diamagnetic behavior with a nearly temperature-independent susceptibility of $\chi = -3(2) \times 10^{-5}$ emu mol^{-1}. The increase in the susceptibility below 50 K (Curie tail) can be attributed to trace amounts of paramagnetic impurities. The intrinsic diamagnetism of $La_3Pt_4Zn_4$ overcompensates the Pauli contribution of the conduction electrons, leading to an overall negative susceptibility in the high-temperature regime.

$La_3Pd_4Zn_4$ exhibits a nearly temperature-independent extremely small susceptibility above 50 K with $\chi = 4(3) \times 10^{-5}$ emu mol^{-1} measured at an externally applied field of 50 kOe. The high standard deviation accounts for the scattering of the data points. The intrinsic diamagnetism and the Pauli contribution almost compensate each other.

Experimental

Syntheses

Starting materials for the syntheses of the $La_3Pd_4Zn_4$ and $La_3Pt_4Zn_4$ samples were lanthanum ingots (Johnson Matthey), palladium and platinum powder (Degussa-Hüls), and zinc granules (Merck), all with stated purities better than

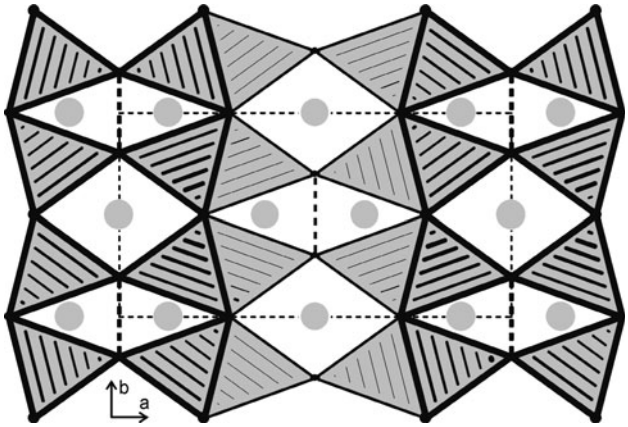

Fig. 2 The network of condensed $ZnPt_{4/4}$ tetrahedra in the structure of $La_3Pt_4Zn_4$

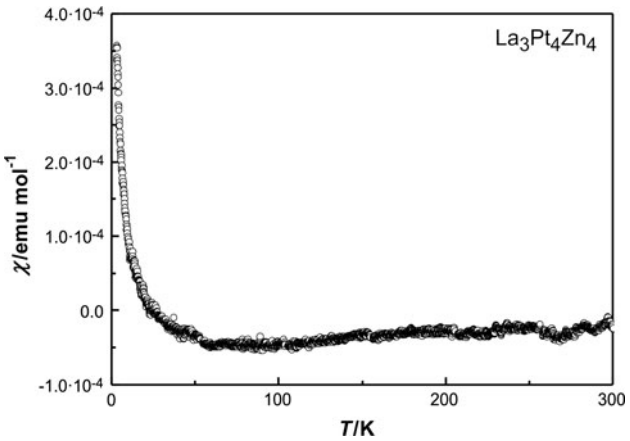

Fig. 3 Temperature dependence of the magnetic susceptibility of $La_3Pt_4Zn_4$ measured at 10 kOe

99.9%. In the first step, pieces of the lanthanum ingots were arc-melted [34] under argon (ca. 700 mbar) to small buttons. The argon was purified before with molecular sieves, silica gel, and titanium sponge (900 K). The elements were then weighed in the ideal 3:4:4 atomic ratios and arc-welded in small tantalum tubes. The tantalum ampoules were then placed in a water-cooled sample chamber of an induction furnace (Hüttinger Elektronik, Freiburg, Typ TIG 1.5/300) [35]. The ampoules were rapidly heated to 1,370 K and kept at that temperature for 5 min, followed by an annealing sequence of 2 h at 1,070 K. The temperature was controlled through a Sensor Therm Metis MS09 pyrometer with accuracy of ±30 K. The samples were then quenched by switching off the power supply. Later the tantalum ampoules were sealed in silica tubes (oxidation protection), annealed at 1,070 K for 6 h, and slowly cooled down to room temperature at a rate of 2 K/h. The brittle, silvery samples could easily be separated from the tantalum tubes. No reaction with the container material was evident. The polycrystalline samples were stable in air over months. Single crystals exhibited metallic luster while ground powder was dark grey.

Scanning electron microscopy

Semiquantitative energy-dispersive X-ray (EDX) analyses of the two single crystals investigated on the diffractometers were carried out with a Zeiss EVO MA10 scanning electron microscope with LaB_6, Pd, Pt, and Zn as standards. The experimentally observed compositions were close to the ideal one. No impurity elements have been observed.

X-ray diffraction data

The $La_3Pd_4Zn_4$ and $La_3Pt_4Zn_4$ samples were characterized by Guinier patterns [image plate system, Fujifilm, BAS-1800, Cu $K\alpha_1$ radiation and α-quartz ($a = 491.30$, $c = 540.46$ pm) as an internal standard]. The orthorhombic lattice parameters were refined on the basis of the powder data using a least-squares routine. Correct indexing was ensured through a comparison with calculated [36] patterns using the positional parameters obtained from the structure refinements.

Single crystals were obtained from the annealed sample by mechanical fragmentation. Selected crystals were glued to quartz fibers using beeswax and were characterized by Laue photographs on a Buerger camera (white molybdenum radiation, image plate technique, Fujifilm, BAS-1800) in order to check their suitability for intensity data collection. A data set of an appropriate $La_3Pd_4Zn_4$ crystal was collected at room temperature by use of a four-circle diffractometer (CAD4) with graphite-monochromatized Ag K_α radiation and a scintillation counter with pulse height discrimination. The scans were taken in $\omega/2\theta$ mode, and an empirical absorption correction was applied on the basis of psi-scan data, accompanied by a spherical absorption correction. The $La_3Pt_4Zn_4$ crystal was measured at room temperature by use of a Stoe IPDS-II image plate system (graphite-monochromatized Mo radiation; $\lambda = 71.073$ pm) in oscillation mode. A numerical absorption correction was applied to the data. All relevant crystallographic data and details of the data collections and evaluations are listed in Table 1.

Details may be obtained from: Fachinformationszentrum Karlsruhe, D-76344 Eggenstein-Leopoldshafen (Germany), by quoting registry nos. CSD-423152 ($La_3Pd_4Zn_4$) and CSD-423153 ($La_3Pt_4Zn_4$).

Magnetic measurements

For magnetic measurements 57.188 mg and 63.118 mg of the polycrystalline $La_3Pt_4Zn_4$ and $La_3Pd_4Zn_4$ samples were

packed in Kapton foil and attached to a sample holder rod. The measurements were performed using the VSM option of a quantum design physical property measurement system (PPMS), in the temperature range of 3–300 K and with magnetic flux densities up to 50 kOe.

Acknowledgments We thank Dipl.-Ing. U. Ch. Rodewald for the intensity data collections. This work was financially supported by the Deutsche Forschungsgemeinschaft. T.M. is indebted to the Forschungsschule Molecules and Materials–A Common Design Principle for a PhD stipend.

References

1. Gschneidner KA Jr, Eyring L, Bünzli J-CG, Pecharsky VK (1978-2011) Handbook on the Physics and Chemistry of Rare Earths. Elsevier, Amsterdam, Volumes 1–41
2. Rodewald UC, Chevalier B, Pöttgen R (2007) J Solid State Chem 180:1720
3. Tappe F, Pöttgen R (2011) Rev Inorg Chem (in press)
4. Hermes W, Al Alam AF, Matar SF, Pöttgen R (2008) Solid State Sci 10:1895
5. Mishra T, Pöttgen R (2011) Intermetallics 19:947
6. Mishra T, Pöttgen R (2011) Z Naturforsch 66b:671
7. Makaryk OYa, Dmytriv GS, Kevorkov DG, Pavlyuk VV (2001) J Alloys Compd 317–318:448
8. Pavlyuk V, Prochwicz W, Solokha P, Zelinska O, Marciniak B, Różycka-Sokołowska E (2006) J Alloys Compd 407:226
9. De Negri S, Solokha P, Saccone A, Pavlyuk V (2008) Intermetallics 16:168
10. Contardi V, Zanicchi G, Marazza R, Ferro R (1983) J Less-Common Met 90:L25
11. Nasch T, Jeitschko W, Rodewald UC (1997) Z Naturforsch 52b:1023
12. Gross N, Nasch T, Jeitschko W (2001) J Solid State Chem 161:288
13. Zelinska OYa, Pavlyuk VV, Zelinskiy AV, Davydov VM (2002) J Alloys Compd 343:132
14. Gross N, Block G, Jeitschko W (2002) Chem Mater 14:2725
15. Mishra R, Hermes W, Rodewald UC, Hoffmann R-D, Pöttgen R (2008) Z Anorg Allg Chem 634:470
16. Eyert V, Scheidt E-W, Scherer W, Hermes W, Pöttgen R (2008) Phys Rev B 78:214420
17. Mishra R, Hermes W, Pöttgen R (2007) Z Naturforsch 62b:1581
18. Dhar SK, Kulkarni R, Hidaka H, Toda Y, Kotegawa H, Kobayashi TC, Manfrinetti P, Provino A (2009) J Phys Condens Matter 21:156001
19. Dhar SK, Kulkarni R, Manfrinetti P, Pani M, Yonezawa Y, Aoki Y (2007) Phys Rev B 76:054411
20. Mishra T, Hermes W, Harmening T, Eul M, Pöttgen R (2009) J Solid State Chem 182:2417
21. Hermes W, Harmening T, Pöttgen R (2009) Chem Mater 21:3325
22. Rieger W (1970) Monathsh Chem 101:449
23. Sheldrick GM (1997) SHELXS-97, Program for the solution of crystal structures, University of Göttingen; (1990) Acta Crystallogr A46:467
24. Sheldrick GM (1997) SHELXL-97, Program for Crystal Structure Refinement, University of Göttingen; (2008) Acta Crystallogr A64:112
25. Villars P, Cenzual K (2010) Pearson's crystal data: crystal structure database for inorganic compounds, release 2009/10, ASM International®. Materials Park, Ohio
26. Miller GJ (1998) Eur J Inorg Chem 523
27. Gelato LM, Parthé E (1987) J Appl Crystallogr 20:139
28. Parthé E, Gelato LM (1984) Acta Crystallogr 40A:69
29. Emsley J (1999) The elements. Oxford University Press, Oxford
30. Niepmann D, Prots' YuM, Pöttgen R, Jeitschko W (2000) J Solid State Chem 154:329
31. Donohue J (1974) The structures of the elements. Wiley, New York
32. Liebrich O, Schäfer H, Weiss A (1970) Z Naturforsch 25b:650
33. Monconduit L, Belin C (1999) Acta Crystallogr C55:1199
34. Pöttgen R, Gulden Th, Simon A (1999) GIT Labor-Fachz 43:133
35. Kußmann D, Hoffmann R-D, Pöttgen R (1998) Z Anorg Allg Chem 624:1727
36. Yvon K, Jeitschko W, Parthé E (1977) J Appl Crystallogr 10:73